

# Fibrillar Self-Organization of a Line-Active Partially Fluorinated Thiol within Binary Self-Assembled Monolayers

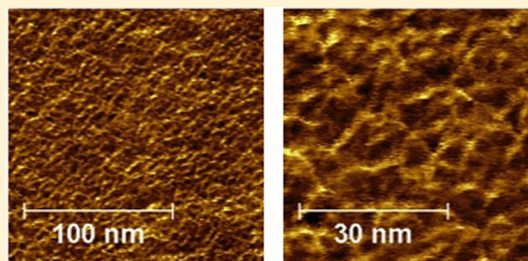
Andrew C. Jamison,<sup>†</sup> Shishan Zhang,<sup>†</sup> Oussama Zenasni,<sup>†</sup> Daniel K. Schwartz,<sup>\*,‡</sup> and T. Randall Lee<sup>\*,†</sup>

<sup>†</sup>Departments of Chemistry and Chemical Engineering and the Texas Center for Superconductivity, University of Houston, Houston, Texas 77204-5003, United States

<sup>‡</sup>Department of Chemical and Biological Engineering, University of Colorado, Boulder, Boulder, Colorado 80309-0596, United States

## Supporting Information

**ABSTRACT:** Self-assembled monolayers (SAMs) were prepared from a novel two-tailed partially fluorinated thiol (F8C11/C16), possessing one hydrocarbon chain and one chain with an extended fluorinated segment, and from mixtures of F8C11/C16 and hexadecanethiol (C16) on gold, with the expectation that the internal chemical dissimilarity and wedge-like shape of F8C11/C16 would lead to unique self-organizational motifs. The SAMs were systematically characterized using ellipsometry, atomic force microscopy (AFM), X-ray photoelectron spectroscopy (XPS), contact angle goniometry, and polarization modulation infrared reflection–absorption spectroscopy (PM-IRRAS). Based on this characterization, the one-component F8C11/C16 SAMs exhibited relatively poor molecular organization compared to traditional alkanethiols, forming low coverage monolayers with significant molecular disorder. However, the series of mixed SAMs formed from F8C11 and F8C11/C16 were anomalously well ordered as indicated by film thickness, surface coverage, and the frequencies of characteristic vibrational modes. AFM images of these mixed SAMs exhibited nanoscale fibrillar structures in a birds-nest morphology, suggesting that in the presence of a C16 matrix, the F8C11/C16 component organized into the two-dimensional analogue of discrete bilayers. Control experiments involving mixed SAMs comprised of F8C11/C16 and a single-tailed partially fluorinated thiol (F8C11) or C16 and F8C11 exhibited no appreciable indication of interesting self-organization beyond an evenly dispersed mixing of the thiolates or phase separation, respectively.



## ■ INTRODUCTION

The development of methods for controlling self-organization and morphology in mixed-adsorbate systems can lead to an increase in the number of applications for self-assembled monolayer (SAM) films in nanoscale devices. The advantages associated with achieving chemically induced ordering of the surface distribution of specifically designed surfactants can be found in the research associated with advanced SAM systems: the preparation of mixed SAMs that allow specific interactions between nanoparticles, enabling unique nanoparticle structures;<sup>1</sup> the isolation of novel SAM adsorbates targeted for use as components in nanoelectronics;<sup>2,3</sup> the creation of nanoscale arrays or specialized biosensors for nanoscale diagnostics;<sup>4</sup> and the possible development of nanoscale circuitry through the careful design of adsorbate structure and equilibrium processes.<sup>5</sup>

Phase control within a three-dimensional (3D) environment to produce specific macroscale characteristics for liquid systems is currently accomplished through the prudent application of a surfactant. In an aqueous solution, the introduction of an appropriate amphiphilic molecule provides the potential for creating micelles that reduce the solution's organizational energy through structural reduction in interfacial tension.<sup>6</sup> In 3D systems, surfactants that lack the ability to provide a significant difference in head-to-tail solubility typically also fail

to create macrostructures such as micelles. Additionally, simple surfactants possessing a polar headgroup with an extended alkyl chain tend to form micelles that are size-limited—they cease growing upon reaching a characteristic size.<sup>6</sup>

The application of surfactant technology to manipulate two-dimensional (2D) phase structures at interfacial boundaries (an array of mixed interfacial surfactants in the form of a monolayer) requires the development of molecules that not only possess a headgroup that forms a stable bond with the substrate but also possess structural features that create strong, reliable, phase-inducing interactions within the monolayer. Examples of phase development within a monolayer film initiated at an air–liquid interface (Langmuir–Blodgett monolayer films, LB films)<sup>7–11</sup> or on a solid substrate (self-assembled monolayers, SAMs)<sup>12–17</sup> abound in the literature. However, few involve the use of an intervening surfactant molecule to direct phase boundary development within the monolayer. For such films, one method of determining the influence of a 2D surfactant upon the phase boundaries that develop between immiscible surface-active molecules is to assess the line tension along those boundaries with and without

Received: July 17, 2012

Revised: November 9, 2012

Published: November 10, 2012

the intervening line-active phase boundary surfactant (“linactant”) present. These specialty surfactants have been defined by Trabelsi and co-workers in their research on line tension within monolayers as those that “partition at phase boundaries and reduce the line tension between coexisting two-dimensional phases in molecular monolayers”.<sup>18</sup>

Previous work by our research team has demonstrated that partially fluorinated compounds can exert a significant influence upon line tension in LB films and monolayers self-assembled on mica.<sup>18,19</sup> Specifically, we compared a single-tailed motif to that of a double-tailed surfactant to determine which more efficiently reduced line tension within a monolayer film. Additionally, various single-tailed linactants, possessing differing lengths for their hydrocarbon and fluorocarbon chain segments, were ranked according to their linactant efficiency.<sup>20</sup>

The focus of the current report is not upon the efficiency of a proposed linactant, but upon the value of this type of unique surfactant in manipulating the nature of the surface structures formed within a SAM. For SAMs prepared on a gold substrate, the structuring of the domains that form is complicated by the presence of the chemical bonds of the headgroups with the solid surface, as compared to Langmuir films where the interaction of the headgroup during phase development is with a fluid substrate. Therefore, the role of line tension on phase boundary development is influenced by the surface’s role in the film-forming processes.<sup>21</sup> The ultimate goal of the research examined in this report is the development of patterned SAMs with well-defined phase domain ordering subject to control through the utilization of adsorbates specifically designed to intervene at phase boundaries, providing a chemical means of creating surface structures via equilibrium methods. This particular study started with the synthesis of a double-tailed surfactant designed to adsorb at a phase boundary: one tail (the alkyl chain) is expected to prefer the aliphatic phase while the other (the partially fluorinated chain) would hypothetically favor a fluorinated phase (see Figure 1).<sup>22</sup>

The fundamental phases for the mixed SAMs are associated with molecules **C16** (hydrocarbon phase) and **F8C11** (fluorocarbon phase). In principle, a mixture of molecule

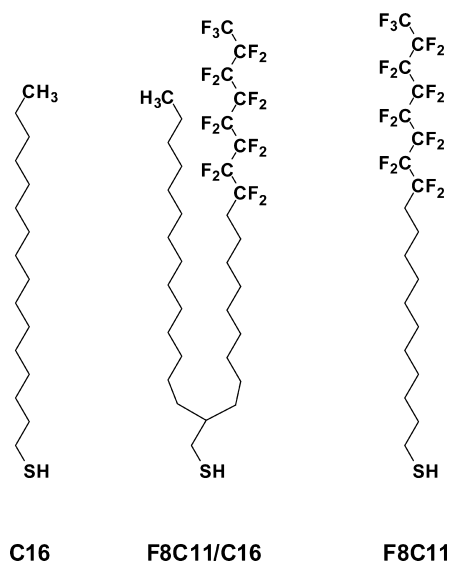


**Figure 1.** Structures for hexadecanethiol (**C16**), the double-tailed partially fluorinated monothiol (**F8C11/C16**), and the corresponding partially fluorinated single-tailed thiol (**F8C11**).

**C16** and **F8C11/C16** could represent a 2D analogue to a micellar phase, producing binary SAMs with independent structures formed from **F8C11/C16**. According to the micelle model, as **F8C11/C16** is introduced and the concentration of **F8C11/C16** is increased, the linactant-directed structures on the surface should increase in population, each structure with a characteristic dimension of two molecules. At higher concentrations, the surface aggregates might become elongated and eventually form long lines as the system adjusts to minimize surface energy.<sup>23</sup> A schematic cross section of a linactant-directed phase structure is illustrated in Figure 2. In this analogy, a three-component mixture of **C16**, **F8C11/C16**, and **F8C11** would represent an emulsion or microemulsion.

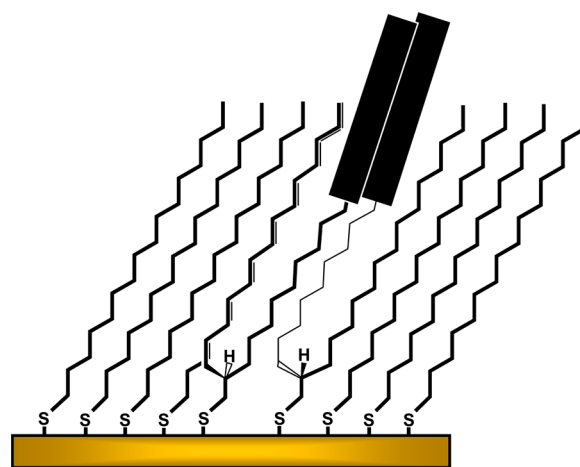


**Figure 2.** Illustration of a cross section of a linactant-directed structure in a binary SAM formed from **C16** and **F8C11/C16**. The black rectangles represent the perfluorinated segments of the **F8C11/C16** adsorbate.

The characterization of SAMs in general, and mixed SAMs in particular, is especially challenging and requires a complementary multitechnique approach.<sup>24–27</sup> While atomic force microscopy (AFM) can be useful for observations of surface topography, it provides little information about the degree of molecular organization, and in fact the utility of this approach is limited in cases where structures are extremely small. Spectroscopic methods provide high sensitivity and quantitative information with respect to molecular order. For example, a recent study by Centrone et al.<sup>28</sup> utilized a previously established relationship between the stretching frequencies of the C–H bonds found in extended alkyl chains and the conformational order of systems containing such chains<sup>29–33</sup> to identify trends in phase development for mixed-monolayer systems on metal nanoparticles. Similarly, Whitesides and colleagues extensively published about the formation and analysis of mixed-monolayer films on flat gold, laying the groundwork for the current analytical methods used in the study of binary SAMs.<sup>25,26,34–36</sup> Vibrational spectroscopy, and complementary methods such as ellipsometry and contact angle goniometry, are particularly useful when used in concert to study the systematic development of molecular order as a function of SAM composition.

An earlier paper from our team focused on the synthesis and characterization of SAMs prepared from compound **F8C11/C16**.<sup>22</sup> The single-component SAMs formed from this adsorbate were compared to those formed from normal

hexadecanethiol, C16, and the partially fluorinated single-chain thiol F8C11. This second report provides a review of the binary SAMs formed with this double-tailed thiol. While limited, there are a few examples of this type of thiol architecture in the literature, but these predecessors were not targeted for phase manipulation.<sup>37–41</sup> For the current study, the three series of mixed-monolayer films were composed of C16 and F8C11/C16, F8C11 and F8C11/C16, along with a reference series composed of C16 and F8C11. Each of these sets of SAMs was prepared with a systematic variance of the relative ratio of the component thiols in the ethanolic developing solution from which the individual SAMs were formed. Analysis of the resulting SAMs was conducted using ellipsometry, contact angle goniometry, polarization modulation infrared reflection–absorption spectroscopy (PM-IRRAS), X-ray photoelectron spectroscopy (XPS), scanning tunneling microscopy (STM), and atomic force microscopy (AFM). Prior to the acquisition of the AFM images, all of the analytical data were consistent with a model in which the mixed SAMs of C16 and F8C11/C16 were producing 2D micelles throughout the entire series of mixed monolayers. However, as described below, the observed unique behavior is also consistent with nanoscale molecular organization of component F8C11/C16 into 2D “bilayers”. The other two series failed to exhibit any particularly interesting behavior and are thus described only briefly.

## EXPERIMENTAL SECTION

**Materials.** The adsorbate 12,12,13,13,14,14,15,15,16,16,17,17,18,18,19,19-heptadecafluorononadecane-1-thiol (F8C11) was prepared according to a procedure available in the literature.<sup>42,43</sup> The synthetic scheme used to produce 12,12,13,13,14,14,15,15,16,16,17,17,18,18,19,19-heptadecafluoro-2-tetradecylnonadecane-1-thiol (F8C11/C16) was given in the initial report on this double-tailed thiol.<sup>22</sup> Hexadecanethiol (C16) was acquired from Alfa Aesar and used as purchased.

Gold (99.999%) was purchased from Kamis Inc., chromium rods (99.9%) from R. D. Mathis Company, and silicon wafers from Silicon Inc. The silicon wafers were 100 mm Si(100) single crystal wafers polished on one side. The rinse solvents, methanol (MeOH) and tetrahydrofuran (THF), were acquired from Mallinckrodt Chemicals. Anhydrous ethanol (EtOH) was purchased from Pharmco-Aaper.

**Preparation of SAMs.** Solutions of the thiol(s) at 1 mM concentration were prepared in ethanol in vials previously cleaned with piranha solution (7:3 concentrated H<sub>2</sub>SO<sub>4</sub>/30% H<sub>2</sub>O<sub>2</sub>). *Caution: piranha solution reacts violently with organic materials and should be handled carefully.* The vials were then rinsed with deionized water, followed by ethanol, and dried in an oven at 100 °C. Gold surfaces were prepared by deposition of a bonding primer of thermally generated chromium vapors (ca. 100 Å) onto ethanol-rinsed Si(100) wafers, followed by vapor deposition of gold (ca. 1000 Å). The resulting gold-coated wafers were cut into slides (~1 × 3 cm), rinsed with absolute ethanol, and blown dry with nitrogen gas prior to immersion in the already prepared thiol solutions. For the ethanolic developing solutions, the surfactant ratios were varied while the overall thiol concentration was maintained at 1.0 mM. The SAMs were allowed to equilibrate for at least 48 h. For each SAM series, six monolayers were prepared with the following development solution ratios (the “solution composition”): 100% A, 80% A with 20% B, 60% A with 40% B, 40% A with 60% B, 20% A with 80% B, and 100% B.

**Measurements of Ellipsometric Thickness.** Thickness measurements for the monolayers were obtained with a Rudolph Research Auto EL III ellipsometer equipped with a He–Ne laser operating at 632.8 nm at an angle of incidence of 70°. To calculate the thicknesses, a refractive index of 1.45 was used for all of the films. For each individual monolayer of the three binary SAM series, data were collected and averaged from at least three measurements on two distinct slides. The

thickness measurements for the SAMs were found to be reproducible within ±2 Å.

**Measurements of Contact Angles.** Contact angle measurements were obtained with a ramé-hart model 100 contact angle goniometer. The contacting liquids that were used were hexadecane (HD; Aldrich, 99+%) and water (W; Milli-Q deionized). A Matrix Technologies micro-Electrapette 25 was utilized for liquid drop dispensing and withdrawal. Contact angle data were collected and averaged for measurements on two distinct slides per each SAM using three separate drops on each slide. Advancing ( $\theta_a$ ) and receding ( $\theta_r$ ) contact angles were taken for both drop edges with the pipet remaining in contact with the drop throughout the procedure.

**Acquisition of X-ray Photoelectron Spectra.** A PHI 5700 X-ray photoelectron spectrometer (XPS) equipped with a monochromatic Al K $\alpha$  X-ray source ( $h\nu = 1486.7$  eV) with an angle of incidence of 90° relative to the axis of a hemispherical energy analyzer was employed to obtain X-ray photoelectron spectra of the SAMs. The instrument was set at a photoelectron takeoff angle of 45° from the surface with a pass energy of 23.5 eV. The base pressure in the chamber during data acquisition was  $\sim 4 \times 10^{-8}$  Torr, and the spectra were collected at room temperature. The binding energies for C<sub>1s</sub>, F<sub>1s</sub>, and S<sub>2p</sub> peaks were referenced to that of the Au<sub>4f 7/2</sub> peak at 84.0 eV.

To calculate the surface compositions of the SAMs generated from the binary mixtures in solution for the two series incorporating C16, the XPS F<sub>1s</sub> to Au<sub>4f</sub> signal ratio for SAMs derived from the pure thiols F8C11/C16 and F8C11 was used to normalize the data for the F<sub>1s</sub> to Au<sub>4f</sub> signal ratio for their respective sets of data. This provides a reliable estimate of the relative surface presence of the fluorinated thiolates as compared to a SAM fully populated with the fluorinated species. To calculate the surface composition for the series incorporating both F8C11/C16 and F8C11, the difference between the two F<sub>1s</sub> to Au<sub>4f</sub> signal ratios for the SAMs prepared from pure thiols F8C11/C16 and F8C11 was used to normalize the data, after each individual ratio for the SAMs in the series were reduced by the F<sub>1s</sub> to Au<sub>4f</sub> signal ratio for F8C11/C16.

Additionally, graphs of the S<sub>2p</sub> to Au<sub>4f</sub> ratios for each series were assembled as a means of analyzing general trends in the data for the relative surface density. For these graphs, the ratio for the single-component SAM possessing the most efficient packing characteristics was used for normalization.

**Acquisition of PM-IRRAS Spectra.** Polarization modulation infrared reflection–absorption spectroscopy (PM-IRRAS) data were collected utilizing a Nicolet Nexus 670 Fourier transform infrared spectrometer equipped with a liquid nitrogen-cooled MCT (mercury–cadmium telluride) detector and a Hinds Instruments PEM-90 photoelastic modulator (37 kHz). The infrared light was reflected off the sample surface at an angle of incidence of 80°. We collected 256 scans to produce each spectrum, with each scan having a spectral resolution of 4 cm<sup>-1</sup>.

**Acquisition of Scanning Tunneling and Atomic Force Microscope Images.** Images were acquired by scanning tunneling microscopy (STM) and atomic force microscopy (AFM) on an Agilent Technologies 5500 scanning probe microscope utilizing interchangeable scanner heads. For AFM, a 10  $\mu$ m scanner head was used operating in either acoustic ac mode or contact mode. The probe was a Bruker MSNL-10 silicon tip on a silicon nitride cantilever. The probe for STM scanning was a platinum–iridium wire cut immediately prior to imaging. The gold surface used to provide high-resolution images was atomically smooth gold on mica from Agilent Technologies.

## RESULTS

**Scanning Probe Microscopy Measurements of Surface Topography.** Figure 3a shows an AFM topographic image for a mixed SAM whose solution composition was 20:80, C16:F8C11/C16. The surface area scanned for this image was  $\sim 325$  nm × 325 nm. A higher magnification image was achieved by probing the surface in ethanol, as shown in Figure 3b. Prior research suggests that the presence of an intervening

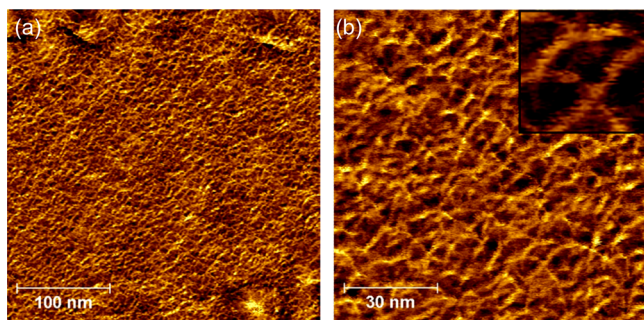


**Figure 3.** AFM images collected in AC (tapping) mode in (a) air and (b) ethanol for a SAM developed in a 20:80 mixed-thiol solution (C16:F8C11/C16). Contrast for the enlarged image inset in the upper right-hand corner of (b) has been enhanced to highlight the suggested phase structures.

liquid such as ethanol reduces adhesive forces between the AFM probe and the interface of the SAM,<sup>44</sup> which might reduce the perturbation of the surface structures and improve the quality of the images acquired by AFM. The change in probe environment did not appear to impact the nature of the observed phase structures. However, the collection of these images in two different environments offers some confidence that the images accurately reflect the nature of the fundamental structure of the adsorbates in these films. We enhanced the contrast of the inset in Figure 3b to highlight the detail of the suggested phase structures. We believe that these structures reflect the alignments illustrated in Figure 2. A qualitative review of the fibrillar surface structures shows that many are  $\sim 10$  nm in length and most are roughly 1 nm wide. However, given the typical size of the AFM probe itself ( $\sim 4$  nm), this estimate of width should be treated as an upper limit.

The structures are disordered and interconnected in a bird's-nest morphology. Efforts to image these structures for SAMs with a lower concentration of F8C11/C16 were unsuccessful, as were efforts to image the SAM shown in Figure 3 by contact mode (AFM) or by scanning tunneling microscopy. However, a mixed SAM comprised of C16 and F8C11 was imaged by both of these methods. In contrast with the fibrillar nanostructures observed for the C16:F8C11/C16 mixture, the nature of the nanoscale phase structures for the C16:F8C11 mixed SAM were approximately circular shapes of various sizes. A representative STM image can be found in the Supporting Information (see Figure S1). Efforts to obtain AFM images of phase structures for mixed SAMs formed from F8C11 and F8C11/C16 were unsuccessful.

**Analysis of Surface Composition Using XPS.** XPS provides an efficient means of obtaining compositional data for SAMs formed on gold.<sup>34,45</sup> In addition to insight into the elemental content, the characterization of the surface bonds, and the presence of surface contaminants,<sup>46,47</sup> XPS is also a useful tool for discerning trends with regards to packing or adsorbate surface density in a series of SAMs.<sup>48</sup> For many studies involving alkanethiols on gold, XPS has been an important instrumental method for determining whether the SAM film is effectively bound to the surface or if the monolayer films contain measurable amounts of oxidized headgroups. For the analytical procedure used in this experiment, unbound thiol distorts the XPS data used to calculate adsorbate surface density, leading to an increase in error in these calculations. Steps taken to ensure that such distortions were avoided with the collected data can be found in the Supporting Information.

To prepare the XPS analyses in this report, the areas under the  $S_{2p}$  peaks for sulfur,  $F_{1s}$  peaks for fluorine, and the  $Au_{4f}$  peaks for gold were used to perform the appropriate calculations as outlined in the Experimental Section.

Figure 4 provides a comparison of the mole fraction of F8C11/C16 in the SAM developing solution versus the mole

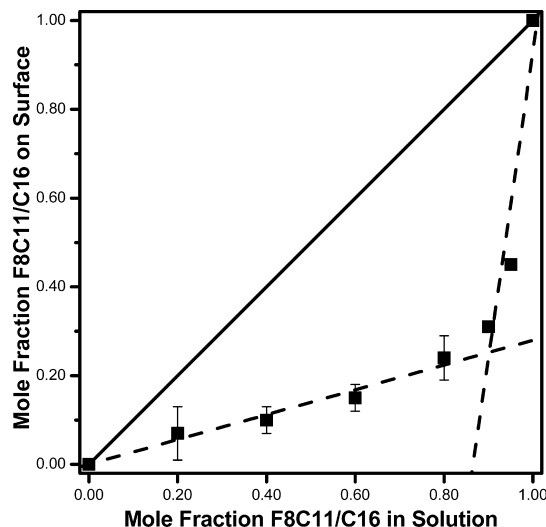


**Figure 4.** Comparison of the mole fraction of F8C11/C16 within the SAM film (y-axis) versus the mole fraction of F8C11/C16 in the SAM developing solution (x-axis) for SAMs comprised of C16 and F8C11/C16, as determined from XPS data. A solid line marks where solution and surface compositions are equivalent. Two dashed lines have been included to enable the estimation of a possible inflection point. Error bars indicate the standard deviation for each of the individual data points.

fraction of F8C11/C16 within the final monolayer film. An important interpretation of these data is that the variance in the adsorbate content of the solution composition versus that of the surface composition reflects a process of competitive adsorption where the dominant adsorbate on the surface is the one with less steric bulk. Variances in surface adsorption related to steric hindrance for similarly structured adsorbates can be found in the work of Bain et al., where a series of thiols and disulfides showed that the thiol was the favored adsorbate by a margin of 2 to 1 over the disulfide.<sup>36</sup> The XPS data in Figure 4 exhibit a clear crossover at a solution composition ratio of  $\sim 10:90$ , C16:F8C11/C16.<sup>49</sup>

A similar adsorption pattern was observed in the XPS data plots for mixed SAMs comprised of F8C11 and F8C11/C16 (see Figure S3a in the Supporting Information), again reinforcing the notion that the double-tailed thiol is the less favored adsorbate. The XPS data for SAMs comprised of C16 and F8C11 (see Figure S3b) appear to indicate a slight preference for F8C11 in the adsorbate surface composition as compared to the solution composition, even though F8C11 is encumbered by a rigid perfluorinated tailgroup. This minor variance in adsorption might be due to stronger van der Waals attractions between the F8C11 adsorbates related to their slightly longer chain length. However, according to Bain and colleagues, such discrepancies in the surface composition of their mixed-SAM systems (where the two adsorbates acted independently and were of similar size) were attributed to solvation effects.<sup>36</sup> For the current system, the relative solubility of the three thiols in ethanol as observed in the preparation of

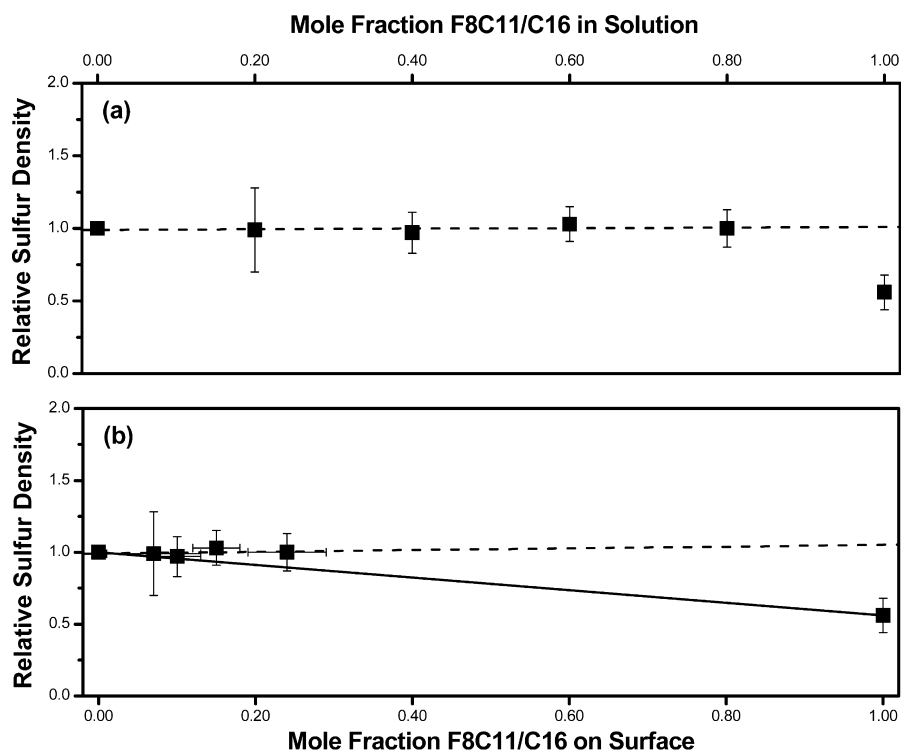


**Figure 5.** The normalized  $S_{2p}$  to  $Au_{4f}$  integrated peak ratios calculated from the XPS data for mixed SAMs comprised of C16 and F8C11/C16. The relative sulfur density (or headgroup density) is normalized using the peak ratio for the single-component SAM formed from C16. The horizontal axis represents the composition of (a) the SAM development solution and (b) the resulting SAM film. A solid line represents an “ideal” trend for the surface adsorbate composition. A dashed line highlights a distinct trend for concentrations of F8C11/C16 less than unity. Error bars indicate the standard deviation for each of the individual data points.

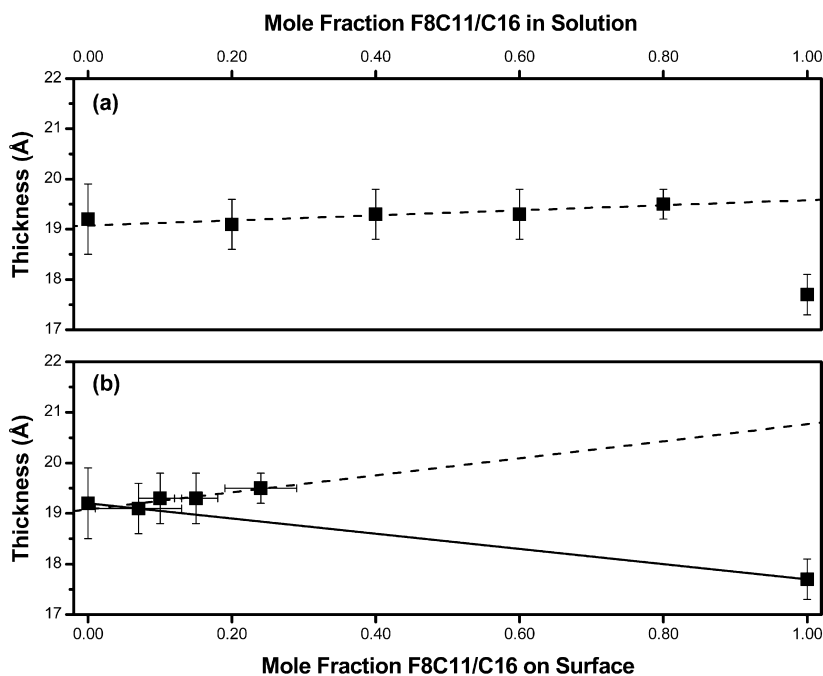


**Figure 6.** Ellipsometric thickness measurements for the mixed SAM series comprised of C16 and F8C11/C16, in angstroms. The horizontal axis represents the composition of (a) the SAM deposition solution and (b) the resulting SAM film. A dashed line emphasizes a distinct trend for concentrations of F8C11/C16 less than unity. A solid line represents an ideal trend for the surface adsorbate composition. Error bars indicate the standard deviation for each of the individual data points.

the deposition solutions is C16 > F8C11/C16 > F8C11. Therefore, the preferred adsorbate apparently reflects the influence of both solvation effects (phase preference) and steric

bulk, with the latter amplified for F8C11/C16 due to the diminished enthalpic gain per chain upon formation of the S–Au bond.

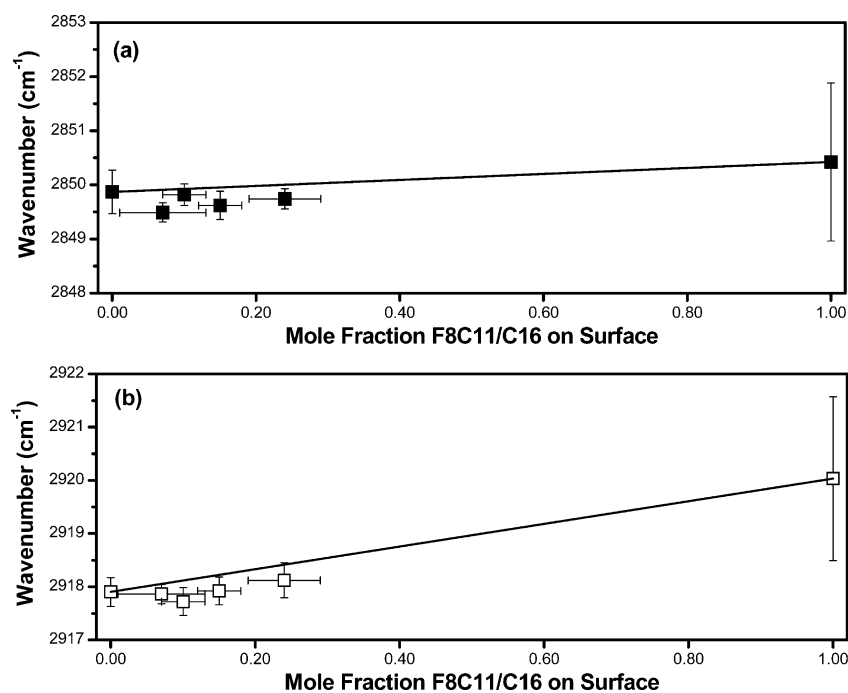


**Figure 7.** PM-IRRAS data for (a) the symmetric (■) and (b) the antisymmetric (□) methylene C–H stretching vibrations for mixed SAMs comprised of C16 and F8C11/C16. The horizontal axes represent the adsorbate composition of the SAMs on the surface. Solid lines represent ideal trends for the surface adsorbate composition. Error bars indicate the standard deviation for each of the individual data points.

The trends for relative thiolate surface density in the form of a normalized relative sulfur density (or headgroup density) are shown in Figure 5 for mixed SAMs comprised of C16 and F8C11/C16, as determined by the mole fraction of F8C11/C16 in the development solution (Figure 5a) and the mole fraction of F8C11/C16 on the surface (Figure 5b). The results of an analysis of the XPS data for the single-component SAMs formed from C16, F8C11/C16, and F8C11 were reported previously.<sup>22</sup> In that report, it was determined that a comparison of the relative adsorbate surface density of these SAMs yielded a general trend of decreasing surface density of C16 > F8C11 > F8C11/C16, a result that is consistent with the data obtained by other instrumental means. As shown in Figure 5, the surface density for all mixed SAMs is the same as for SAMs comprised of C16. The surface density for one-component SAMs comprised of F8C11/C16 is approximately half that of the SAM formed from the single-tailed normal alkanethiol. This result is a logical consequence of the two-tailed structure/stoichiometry of F8C11/C16. However, the absence of a significant decrease in thiolate headgroup density for mixed films indicates the presence of an anomalously high packing density of F8C11/C16 in mixed films relative to that within one-component films. Analogous surface density data for the other mixed SAM series are presented in the Supporting Information (see Figure S4). In both cases, the XPS data are more consistent with an “ideal” mean-field trendline between the two single-component SAMs: the solid line present in Figure 5b and in Figures S4b and S4d in the Supporting Information.

**Ellipsometric Thickness Measurements.** The application of ellipsometry to follow trends in the thickness profile of a series of SAMs provides useful information only because of the height differences for the components of these adsorbed films, providing an indirect means for tracking surface phase development. Assuming the systematic mixing of each SAM

series occurs with a distribution of phase structures of unchanging dimensions, but methodically varying surface population, as the deposition solution mixture for each SAM in the series systematically shifts from one adsorbate mixture to another, then the anticipated trend for a graph of the ellipsometric measurements for the mixed-SAM series would be linear.<sup>6</sup> As shown in Figure 6, for mixed SAMs of C16 and F8C11/C16, the ellipsometric thickness measurements exhibit a linear trend for most of the SAMs in the series.<sup>50</sup> This linear data trend has been highlighted by the inclusion of dashed lines in the figure and provides a notable deviation from an ideal mean-field trendline, the solid line in Figure 6b.<sup>51</sup> The analytical data as a function of the solution composition, such as those in Figure 6a, provide a means of analyzing the relative positioning of the collected data points absent the compression of the mixed-SAM surface composition data and any error associated with the analysis of the XPS data.

The drop in thickness for the last data point is associated with the SAM formed exclusively from F8C11/C16, which Zhang and co-workers have previously determined forms a loosely packed SAM.<sup>22</sup> As discussed further below, the discrepancy of this last data point with respect to the trend associated with the other concentrations (a distinct drop in film thickness in contrast with the gradual increase observed for lower concentrations) constitutes direct evidence for a qualitatively different type of organization of compound F8C11/C16 within mixed SAMs versus within a one-component SAM. The data for the other two series of mixed SAMs failed to exhibit consistent trends as shown in the Supporting Information (see Figure S5). The ellipsometric data for the single-component SAMs are consistent with published data.<sup>22,40,52</sup>

**SAM Organization Analyzed by PM-IRRAS.** As mentioned above, the band positions of the C–H stretching vibrations observed via infrared spectroscopy are known as

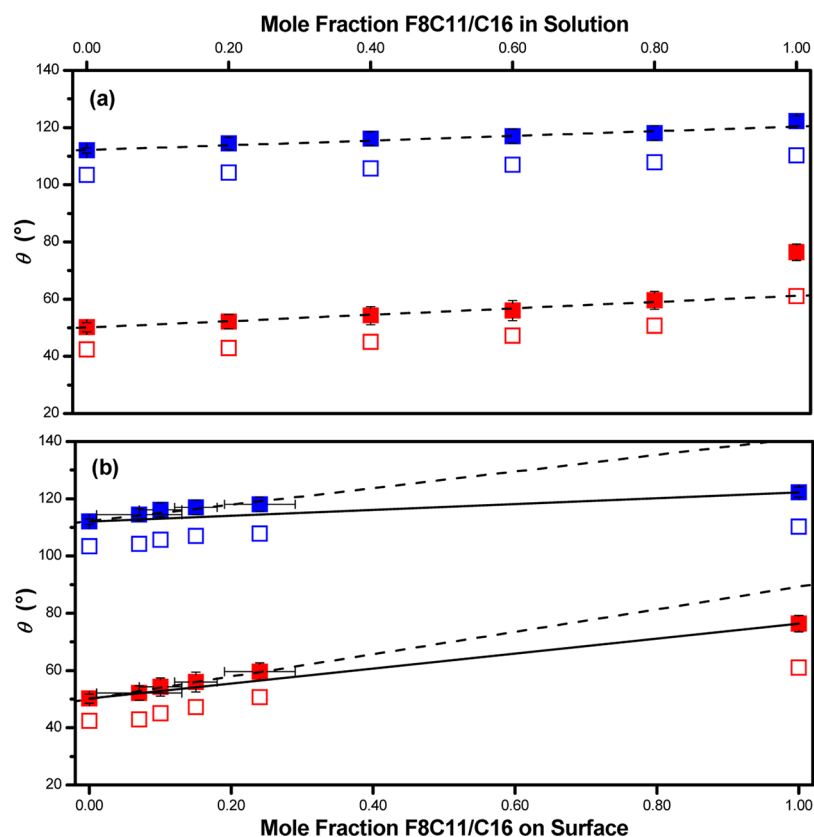


**Figure 8.** Wettability data for contacting liquids on mixed SAMs comprised of C16 and F8C11/C16 for water for advancing (blue ■) and receding (blue □) contact angles ( $\theta$ ) and hexadecane for advancing (red ■) and receding (red □) contact angles. The horizontal axis represents the composition of (a) the SAM development solution and (b) the resulting SAM film. Solid lines represent ideal trends for the surface adsorbate composition. Dashed lines highlight distinct trends for the advancing contact angles for concentrations of F8C11/C16 less than unity. Error bars indicate the standard deviation for each of the individual data points.

sensitive indicators of the molecular environment of the alkyl chains in a SAM and also of the nature of the collective conformational order of the individual chains.<sup>30,53</sup> Previous studies of normal alkanethiolate SAMs have shown that the relative crystallinity for alkyl chains in a self-assembled monolayer film can be estimated from the band position of the methylene C–H antisymmetric vibration ( $\nu_a^{\text{CH}_2}$ ) and symmetric vibration ( $\nu_s^{\text{CH}_2}$ ).<sup>29,32,33</sup> This determination was made by comparison to the IR spectral data collected for  $\nu_a^{\text{CH}_2}$  of a set of solid *n*-alkanes ( $\sim 2920\text{ cm}^{-1}$ ) versus liquid *n*-alkanes ( $\sim 2928\text{ cm}^{-1}$ ) and for  $\nu_s^{\text{CH}_2}$  of solid *n*-alkanes ( $\sim 2850\text{ cm}^{-1}$ ) versus liquid *n*-alkanes ( $\sim 2856\text{ cm}^{-1}$ ).<sup>30</sup> The importance of these peak positions with regards to determining the relative structural order of a variety of alkyl chain assemblies was also confirmed in Raman studies involving polymethylene chains.<sup>54,55</sup>

The PM-IRRAS data collected for mixed SAMs comprised of C16 and F8C11/C16 are displayed in Figure 7.<sup>56</sup> For this study, both the  $\nu_s^{\text{CH}_2}$  (Figure 7a) and  $\nu_a^{\text{CH}_2}$  (Figure 7b) peak positions were reviewed to determine if they provided indications of changes in molecular environment for the methylene units. For both modes, the peak positions are essentially unchanged within experimental error for all mixed films but exhibit a distinct jump to greater wavenumbers for one-component SAMs of compound F8C11/C16. This phenomenon is particularly apparent for  $\nu_a^{\text{CH}_2}$  but also discernible for  $\nu_s^{\text{CH}_2}$ . Consistent with the interpretation of the ellipsometric data described above, this behavior is again direct

evidence that the organization of F8C11/C16 within mixed SAMs (with C16) is qualitatively different than the organization within one-component films. In particular, F8C11/C16 is conformationally disorganized within one-component films but fails to induce disorder within this series of mixed films.

The plots for the PM-IRRAS data as a function of the mole fraction of F8C11/C16 in the development solution are shown in the Supporting Information in Figure S6. Figure S7 provides a representative set of spectra for the SAMs of the series prepared from C16 and F8C11/C16. Peak positions for the other mixed SAM series are presented in Figures S8 and S9. Interestingly, for mixed SAMs comprised of F8C11 and F8C11/C16, the peak position of  $\nu_a^{\text{CH}_2}$  exhibits a distinct shift between two-component and one-component films of F8C11/C16; however, this is completely absent in the peak positions of  $\nu_s^{\text{CH}_2}$ . Peak positions associated with SAMs comprised of C16 and F8C11 are basically consistent with expected ideal trendlines.

**Film Wettability.** Contact angle goniometry is a useful instrumental method for analyzing the surface composition, relative surface packing, and general ordering of a self-assembled monolayer film.<sup>57</sup> For the current set of mixed-SAM systems, the absolute interpretation of the results obtained from contact angle measurements is complicated by the adsorbate mixture itself. This complication can be attributed, in part, to the added complexity introduced by the double-tailed thiolate, along with irregularities in the interfacial

profile related to the presence of the longer terminal perfluorocarbon segments on **F8C11/C16** and **F8C11** that can protrude above the nonfluorinated alkyl chains. The nanoscale roughness associated with these perfluorinated segments might lead to an exaggerated impact for the terminal perfluorocarbons upon the measured contact angles.<sup>58</sup> However, the associated trends in wettability should correlate with the relative presence of the two types of surface chains for each SAM series. For the SAMs in this study, the dipole associated with the transition between the fluorocarbon and hydrocarbon segments of the adsorbates is sufficiently buried to avoid impacting the surface energy of the SAMs involved.<sup>59</sup> Owing to the absence of any exposed polar component, the surface forces acting on the contacting liquids are limited to dispersive forces.

Advancing contact angles ( $\theta_a$ ) and receding contact angles ( $\theta_r$ ) for the contacting liquids hexadecane (HD; a nonpolar liquid) and water (W; a polar liquid) for SAMs comprised of **C16** and **F8C11/C16** are shown in Figure 8.<sup>60</sup> Solid lines representing an ideal trendline have been inserted in Figure 8b between the  $\theta_a$  data points associated with the two single-component monolayers, providing a guide for analysis of the data for each contacting liquid.

In Figure 8, the blue symbols represent the advancing (solid blue symbols) and receding (unfilled blue symbols) contact angles for W. Consistent with our observations with the relative headgroup density and ellipsometric thickness data, the two-component monolayers in Figure 8b exhibit a distinct trend with composition (indicated by the dashed lines). However, this trend does not extrapolate to a value consistent with that observed for the one-component **F8C11/C16** SAM, again suggesting that the organization of **F8C11/C16** within two-component films is qualitatively different than that within the disordered one-component **F8C11/C16** SAMs.

As for the contact angle data for HD, the red symbols represent the advancing (solid red symbols) and receding (unfilled red symbols) contact angles. The HD contact angle data reflects the greater affinity of the hydrocarbon contacting liquid for the hydrocarbon chains in the mixed SAMs and a measurably lower affinity for the fluorocarbon moieties.<sup>61</sup> The absence of a similar relationship for these adsorbates with W is reflected in the lower slope of the ideal trendline for W. As with W, a distinct trend for the HD  $\theta_a$  data in Figure 8b is highlighted by a dashed line, a trendline associated with the first five data points, that diverges significantly from the ideal trendline. The consistent presence of a linear trend associated with the mixed SAMs for the wettability data collected for these films further supports a conclusion that they are a consequence of a unique structural organization of **F8C11/C16** within the two-component films.

Contact angle data for the other series are presented and described in greater detail in the Supporting Information (see Figure S10). Generally speaking, mixed SAMs comprised of **F8C11** and **F8C11/C16** exhibited contact angles in reasonable agreement with the ideal trendline, which might indicate mixing of the thiolates at the molecular level, while mixed SAMs comprised of **C16** and **F8C11** exhibited trends consistent with significant heterogeneity caused by phase separation.

## DISCUSSION

The results presented above describe a scenario where the two-tailed compound, **F8C11/C16**, forms a low-density poorly ordered SAM on its own but is highly organized within a mixed

SAM with a one-tailed hydrocarbon component (**C16**). Measurements on these mixed SAMs deviate from expectations based on a simple weighted average of two components and exhibit a distinct correlation of trends for the analytical data obtained from a variety of instrumental methods. AFM images suggest that the organization takes the form of extremely narrow fibrillar nanostructures. Analytical data for the mixed SAMs comprised of **F8C11/C16** and the single-tailed partially fluorinated compound (**F8C11**) exhibit trends indicating that the methodical replacement of **F8C11** with **F8C11/C16** in the set of mixed-SAM solutions examined in this paper led to minimal changes in the obtained measurements. However, this series does not afford the continuity in data trends exhibited by the SAMs formed from **C16** and **F8C11/C16**. Recent research on monolayers of fluorocarbon/hydrocarbon (FnHn) diblock moieties indicate that such molecular structures have a strong propensity to self-assemble, a characteristic that is attributed in part to the dipole at the structural transition.<sup>62</sup> These favorable molecular attractions between the fluorocarbon/hydrocarbon segments of the **F8C11** and **F8C11/C16** adsorbates might produce a more intimate intermixing of these components, as compared to **C16** and **F8C11/C16**, leading to the difficulties experienced in attempts to obtain AFM images of surface structures for this series of mixed SAMs. Mixed SAMs of the two single-tailed compounds appear to phase separate into small domains of varying size, and measurements are generally consistent with this spatial heterogeneity.

These observations are entirely consistent with a picture that is in direct analogy with surfactant (e.g., phospholipid) self-assembly in 3D solutions, where **F8C11/C16** corresponds to the surfactant, and **C16** and **F8C11** correspond to two chemically dissimilar solvents (e.g., oil and water). For example, depending on the hydrophilic–lipophilic balance (HLB) of a given surfactant,<sup>63</sup> the surfactant will spontaneously organize into well-defined assemblies (e.g., spherical micelles, cylindrical micelles, or bilayers) in one solvent (as **F8C11/C16** does when dissolved in **C16**) but will be highly soluble in a complementary solvent (as **F8C11/C16** is in **F8C11**). Clearly, the two solvents themselves will engage in uncontrolled phase separation when mixed (i.e., **C16** and **F8C11**). Again for 3D surfactant solutions, it is generally accepted that the morphology of the assembly that is formed in a given case depends on the details of the molecular architecture, specifically, the shape of the surfactant molecule often characterized by the molecular shape factor.<sup>64</sup> Thus, while wedge-shaped surfactants may prefer to assemble into spherical micelles, two-tailed “cylindrical” surfactants such as phospholipids typically assemble into bilayer-based aggregates such as vesicles. Since the cross section of self-assembled surfactant aggregates in 3D always involve some sort of bilayer motif, they exhibit at least one dimension that is associated with twice the molecular length (e.g., 3–5 nm).

In a recent report by Malone and co-workers utilizing partially fluorinated phosphonic acid surfactants within a matrix of a fatty acid LB monolayer, inactant surface structures were characterized in the form of clusters that developed to a characteristic size and shape.<sup>65</sup> They proposed that this system represented the 2D thermodynamic analogue of a micellar dispersion and that the rather large size of the aggregates (tens of nanometers) was due to a splayed configuration associated with the bulky fluorinated tailgroups, as opposed to a bilayer motif as expected in 3D. Objects of similar size had been previously observed in neat monolayers comprised of partially

fluorinated compounds.<sup>19,20</sup> However, as in 3D, it is expected that the size and shape of preferred aggregates will be related to the details of the molecular geometry.

In 2D, symmetry dictates the possibility of two fundamental classes of embedded geometrical manifolds: for example, circular (zero dimensional) and linear (one-dimensional). We propose that the aggregates formed by F8C11/C16 within a matrix of C16 represent an example of a one-dimensional (fibrillar) aggregate in a 2D (monolayer) environment. Interestingly, in contrast with circular aggregates previously observed that had characteristic dimensions an order of magnitude larger than the relative molecular length scale (i.e., the molecular cross section), the fibrils observed here have a width that is consistent with twice the molecular cross section. Additional influences on the final form of the shapes adopted by these assemblies likely include the relative size and conformational mobility of the two phase-incompatible tailgroups. For concreteness, Figure 9 shows a proposed “top-

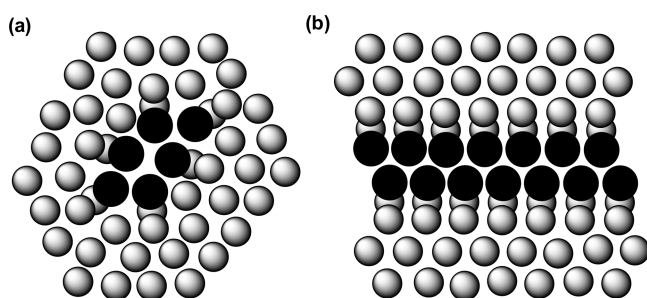


**Figure 9.** Illustration of self-assembled aggregates expected to form in two-component mixtures prepared from a single-tailed and a double-tailed adsorbate: (a) 2D micelles and (b) 2D bilayers.

view” schematic diagram of how compound F8C11/C16 might self-assemble into hypothetical “circular” or linear micelles; the latter is consistent with the observations presented here. We hypothesize that the “side-by-side” geometry of the chemically dissimilar moieties in F8C11/C16 enhances the propensity for this particular type of aggregate to form in the C16 matrix.

## CONCLUSIONS

The design and synthesis of a novel two-tailed partially fluorinated thiol, a linactant possessing one hydrocarbon chain and one chain with an extended fluorinated segment, has revealed unique self-organizational motifs when used in combination with hexadecanethiol in a series of mixed SAMs. The resulting two-component monolayers were anomalously well ordered, as compared to the corresponding single-component films. Additionally, the analytical data associated with this series of mixed SAMs consistently exhibited linear trends as a function of composition, consistent with an increasing concentration of nanoscale structures of unchanging dimension and internal organization. The literature is replete with examples of the challenges involved in designing reliable mixed-monolayer systems for macromolecule attachment, addressing key issues related to monolayer formation such as creating densely packed films,<sup>66</sup> establishing thiol ratios for calibrating attachment sites,<sup>67</sup> or addressing steric crowding problems at the macromolecule attachment site due to the relative thiolate ratio.<sup>68</sup> Ultimately, the unique nanoscale structures uncovered by the data trends for the mixed SAMs formed from C16 and F8C11/C16 might encourage the

development of similarly designed adsorbates, yielding an efficient method for calibrating the density of macromolecule binding sites in mixed-monolayer systems. Such an adsorbate system, with predictable dispersive character, might prove useful in the development of nanoparticle therapeutic and drug delivery systems.<sup>69</sup> Additionally, continued refinement of the architecture of F8C11/C16 might lead to greater control of the resulting phase structures for mixed-thiolate SAMs, possibly leading to reproducible surface structures such as nanoscale lines and uniform circles, providing a chemical means of forming nanoscale architecture for nanoelectronic devices. Future work with this linactant will include analysis of how this double-tailed thiol performs in a ternary mixed-monolayer system.

## ASSOCIATED CONTENT

### Supporting Information

Additional characterization data and analysis of the mixed SAMs (STM image, XPS data, ellipsometric thicknesses, PM-IRRAS data and spectra, and contact angles of water and hexadecane) are presented in Figures S1–S10. This material is available free of charge via the Internet at <http://pubs.acs.org>.

## AUTHOR INFORMATION

### Corresponding Author

\*E-mail: [daniel.schwartz@colorado.edu](mailto:daniel.schwartz@colorado.edu) (D.K.S.); [trlee@uh.edu](mailto:trlee@uh.edu) (T.R.L.).

### Notes

The authors declare no competing financial interest.

## ACKNOWLEDGMENTS

We thank the National Science Foundation (DMR-0906727 to T.R.L. and DMR-0906735 to D.K.S.) and the Robert A. Welch Foundation (E-1320) for generous support. Additionally, Dr. Song Xu of Agilent Technologies provided valuable assistance with our efforts to produce the scanning probe microscopy images presented in this paper.

## REFERENCES

- (1) DeVries, G. A.; Brunnbauer, M.; Hu, Y.; Jackson, A. M.; Long, B.; Neltner, B. T.; Uzun, O.; Wunsch, B. H.; Stellacci, F. Divalent metal nanoparticles. *Science* **2007**, *315*, 358–361.
- (2) Reed, M. A.; Chen, J.; Rawlett, A. M.; Price, D. W.; Tour, J. M. Molecular random access memory cell. *Appl. Phys. Lett.* **2001**, *78*, 3735–3737.
- (3) Majumdar, N.; Gergel-Hackett, N.; Bean, J. C.; Harriott, L. R.; Pattanaik, G.; Zangari, G.; Yao, Y.; Tour, J. M. The electrical behavior of nitro oligo (phenylene ethynylene)s in pure and mixed monolayers. *J. Electron. Mater.* **2006**, *35*, 140–146.
- (4) Mir, M.; Alvarez, M.; Azzaroni, O.; Knoll, W. Comparison of different supramolecular architectures for oligonucleotide biosensing. *Langmuir* **2008**, *24*, 13001–13006.
- (5) Ma, H.; Zin, M. T.; Zareie, M. H.; Kang, M.-S.; Kang, S.-H.; Kim, K.-S.; Reed, B. W.; Behar, C. T.; Sarikaya, M.; Jen, A. K. Y. Assembly of nanomaterials through highly ordered self-assembled monolayers and peptide-organic hybrid conjugates as templates. *J. Nanosci. Nanotechnol.* **2007**, *7*, 2549–2566.
- (6) Evans, D. F.; Wennerstrom, H. *The Colloidal Domain: Where Physics, Chemistry, Biology, and Technology Meet*; 2nd ed.; Wiley-VCH: New York, 1999.
- (7) Sparr, E.; Ekelund, K.; Engblom, J.; Engstroem, S.; Wennerstroem, H. An AFM study of lipid monolayers. 2. Effect of cholesterol on fatty acids. *Langmuir* **1999**, *15*, 6950–6955.
- (8) Shibata, O.; Yamamoto, S. K.; Lee, S.; Sugihara, G. Mixed monolayer properties of tetradecanoic acid with n-perfluorocarboxylic

acids with 10, 12, 14, 16, and 18 carbon atoms. *J. Colloid Interface Sci.* **1996**, *184*, 201–208.

(9) Shibata, O.; Krafft, M. P. Mixed Langmuir monolayers made from single-chain perfluoroalkylated amphiphiles. *Langmuir* **2000**, *16*, 10281–10286.

(10) Solletti, J. M.; Botreau, M.; Sommer, F.; Tran Minh, d.; Celio, M. R. Characterization of mixed miscible and nonmiscible phospholipid Langmuir-Blodgett films by atomic force microscopy. *J. Vac. Sci. Technol., B* **1996**, *14*, 1492–1497.

(11) Ekelund, K.; Sparr, E.; Engblom, J.; Wennerstroem, H.; Engstroem, S. An AFM study of lipid monolayers. 1. Pressure-induced phase behavior of single and mixed fatty acids. *Langmuir* **1999**, *15*, 6946–6949.

(12) Stranick, S. J.; Atre, S. V.; Parikh, A. N.; Wood, M. C.; Allara, D. L.; Winograd, N.; Weiss, P. S. Nanometer-scale phase separation in mixed composition self-assembled monolayers. *Nanotechnology* **1996**, *7*, 438–442.

(13) Ishida, T.; Mizutani, W.; Choi, N.; Ogiso, H.; Azehara, H.; Hokari, H.; Akiba, U.; Fujihira, M.; Kojima, I.; Tokumoto, H. Low dimensional structure formation in self-assembled monolayers on Au(111). *Colloids Surf., A* **1999**, *154*, 219–225.

(14) Ishida, T.; Mizutani, W.; Tokumoto, H.; Hokari, H.; Azehara, H.; Fujihira, M. Nanowire formation in self-assembled monolayers from fluorocarbon-hydrocarbon on Au(111). *Appl. Surf. Sci.* **1998**, *130–132*, 786–791.

(15) Hayes, W. A.; Kim, H.; Yue, X.; Perry, S. S.; Shannon, C. Nanometer-scale patterning of surfaces using self-assembly chemistry. 2. Preparation, characterization, and electrochemical behavior of two-component organothiol monolayers on gold surfaces. *Langmuir* **1997**, *13*, 2511–2518.

(16) Kakiuchi, T.; Sato, K.; Iida, M.; Hobara, D.; Imabayashi, S.; Niki, K. Phase separation of alkanethiol self-assembled monolayers during the replacement of adsorbed thiolates on Au(111) with thiols in solution. *Langmuir* **2000**, *16*, 7238–7244.

(17) Brewer, N. J.; Leggett, G. J. Chemical Force microscopy of mixed self-assembled monolayers of alkanethiols on gold: Evidence for phase separation. *Langmuir* **2004**, *20*, 4109–4115.

(18) Trabelsi, S.; Zhang, S.; Lee, T. R.; Schwartz, D. K. Linactants: surfactant analogues in two dimensions. *Phys. Rev. Lett.* **2008**, *100*, 037802/1–037802/4.

(19) Trabelsi, S.; Zhang, S.; Zhang, Z.; Lee, T. R.; Schwartz, D. K. Semi-fluorinated phosphonic acids form stable nanoscale clusters in Langmuir-Blodgett and self-assembled monolayers. *Soft Matter* **2009**, *5*, 750–758.

(20) Trabelsi, S.; Zhang, Z.; Zhang, S.; Lee, T. R.; Schwartz, D. K. Correlating linactant efficiency and self-assembly: Structural basis of line activity in molecular monolayers. *Langmuir* **2009**, *25*, 8056–8061.

(21) Knobler, C. M.; Schwartz, D. K. Langmuir and self-assembled monolayers. *Curr. Opin. Colloid Interface Sci.* **1999**, *4*, 46–51.

(22) Zhang, S.; Jamison, A. C.; Schwartz, D. K.; Lee, T. R. Self-assembled monolayers derived from a double-chained monothiol having chemically dissimilar chains. *Langmuir* **2008**, *24*, 10204–10208.

(23) Fung, B. M.; Mamrosh, D. L.; O'Rear, E. A.; Frech, C. B.; Afzal, J. Unusual micellar properties of a new class of fluorinated nonionic surfactants. *J. Phys. Chem.* **1988**, *92*, 4405–4411.

(24) Venkataraman, N. V.; Zürcher, S.; Spencer, N. D. Order and composition of methyl-carboxyl and methyl-hydroxyl surface-chemical gradients. *Langmuir* **2006**, *22*, 4184–4189.

(25) Bain, C. D.; Whitesides, G. M. Formation of monolayers by the coadsorption of thiols on gold: variation in the length of the alkyl chain. *J. Am. Chem. Soc.* **1989**, *111*, 7164–7175.

(26) Bain, C. D.; Whitesides, G. M. Correlations between wettability and structure in monolayers of alkanethiols adsorbed on gold. *J. Am. Chem. Soc.* **1988**, *110*, 3665–3666.

(27) Patole, S. N.; Baddeley, C. J.; O'Hagan, D.; Richardson, N. V. Reversible exchange of self-assembled monolayers of semifluorinated n-alkanethiols and n-alkanethiols on Au/mica surfaces. *J. Phys. Chem. C* **2008**, *112*, 13997–14000.

(28) Centrone, A.; Hu, Y.; Jackson, A. M.; Zerbi, G.; Stellacci, F. Phase separation on mixed-monolayer-protected metal nanoparticles: a study by infrared spectroscopy and scanning tunneling microscopy. *Small* **2007**, *3*, 814–817.

(29) Bensebaa, F.; Ellis, T. H.; Badia, A.; Lennox, R. B. Probing the different phases of self-assembled monolayers on metal surfaces: Temperature dependence of the C-H stretching modes. *J. Vac. Sci. Technol., A* **1995**, *13*, 1331–1336.

(30) Snyder, R. G.; Strauss, H. L.; Elliger, C. A. Carbon-hydrogen stretching modes and the structure of n-alkyl chains. 1. Long, disordered chains. *J. Phys. Chem.* **1982**, *86*, 5145–5150.

(31) Laibinis, P. E.; Whitesides, G. M.; Allara, D. L.; Tao, Y. T.; Parikh, A. N.; Nuzzo, R. G. Comparison of the structures and wetting properties of self-assembled monolayers of n-alkanethiols on the coinage metal surfaces, copper, silver, and gold. *J. Am. Chem. Soc.* **1991**, *113*, 7152–7167.

(32) Bensebaa, F.; Ellis, T. H.; Badia, A.; Lennox, R. B. Thermal treatment of n-alkanethiolate monolayers on gold, as observed by infrared spectroscopy. *Langmuir* **1998**, *14*, 2361–2367.

(33) Porter, M. D.; Bright, T. B.; Allara, D. L.; Chidsey, C. E. D. Spontaneously organized molecular assemblies. 4. Structural characterization of n-alkyl thiol monolayers on gold by optical ellipsometry, infrared spectroscopy, and electrochemistry. *J. Am. Chem. Soc.* **1987**, *109*, 3559–3568.

(34) Bain, C. D.; Biebuyck, H. A.; Whitesides, G. M. Comparison of self-assembled monolayers on gold: coadsorption of thiols and disulfides. *Langmuir* **1989**, *5*, 723–727.

(35) Bain, C. D.; Whitesides, G. M. Formation of two-component surfaces by the spontaneous assembly of monolayers on gold from solutions containing mixtures of organic thiols. *J. Am. Chem. Soc.* **1988**, *110*, 6560–6561.

(36) Bain, C. D.; Evall, J.; Whitesides, G. M. Formation of monolayers by the coadsorption of thiols on gold: Variation in the head group, tail group, and solvent. *J. Am. Chem. Soc.* **1989**, *111*, 7155–7164.

(37) Shon, Y.-S.; Lee, S.; Perry, S. S.; Lee, T. R. The adsorption of unsymmetrical spiroalkanedithiols onto gold affords multi-component interfaces that are homogeneously mixed at the molecular level. *J. Am. Chem. Soc.* **2000**, *122*, 1278–1281.

(38) Shon, Y.-S.; Lee, S.; Colorado, R., Jr.; Perry, S. S.; Lee, T. R. Spiroalkanedithiol-based SAMs reveal unique insight into the wettabilities and frictional properties of organic thin films. *J. Am. Chem. Soc.* **2000**, *122*, 7556–7563.

(39) Chechik, V.; Schoenherr, H.; Vancso, G. J.; Stirling, C. J. M. Self-Assembled monolayers of branched thiols and disulfides on gold: Surface coverage, order and chain orientation. *Langmuir* **1998**, *14*, 3003–3010.

(40) Garg, N.; Lee, T. R. Self-assembled monolayers based on chelating aromatic dithiols on gold. *Langmuir* **1998**, *14*, 3815–3819.

(41) Garg, N.; Friedman, J. M.; Lee, T. R. Adsorption profiles of chelating aromatic dithiols and disulfides: Comparison to those of normal alkanethiols and disulfides. *Langmuir* **2000**, *16*, 4266–4271.

(42) Graupe, M.; Koini, T.; Wang, V. Y.; Nassif, G. M.; Colorado, R., Jr.; Villazana, R. J.; Dong, H.; Miura, Y. F.; Shmakova, O. E.; Lee, T. R. Terminally perfluorinated long-chain alkanethiols. *J. Fluorine Chem.* **1999**, *93*, 107–115.

(43) Frey, S.; Heister, K.; Zharnikov, M.; Grunze, M.; Tamada, K.; Colorado, R., Jr.; Graupe, M.; Shmakova, O. E.; Lee, T. R. Structure of self-assembled monolayers of semifluorinated alkanethiols on gold and silver substrates. *Isr. J. Chem.* **2000**, *40*, 81–97.

(44) Yang, Y.; Jamison, A. C.; Barriet, D.; Lee, T. R.; Ruths, M. Odd-even effects in the friction of self-assembled monolayers of phenyl-terminated alkanethiols in contacts of different adhesion strengths. *J. Adhes. Sci. Technol.* **2010**, *24*, 2511–2529.

(45) Ballav, N.; Terfort, A.; Zharnikov, M. Mixing of nonsubstituted and partly fluorinated alkanethiols in a binary self-assembled monolayer. *J. Phys. Chem. C* **2009**, *113*, 3697–3706.

- (46) Castner, D. G.; Hinds, K.; Grainger, D. W. X-ray photoelectron spectroscopy sulfur 2p study of organic thiol and disulfide binding interactions with gold surfaces. *Langmuir* **1996**, *12*, 5083–5086.
- (47) Duwez, A.-S. Exploiting electron spectroscopies to probe the structure and organization of self-assembled monolayers: a review. *J. Electron Spectrosc. Relat. Phenom.* **2004**, *134*, 97–138.
- (48) Rittikulsittichai, S.; Jamison, A. C.; Lee, T. R. Self-assembled monolayers derived from alkoxyphenylethanethiols having one, two, and three pendant chains. *Langmuir* **2011**, *27*, 9920–9927.
- (49) Most of the XPS data presented in Figures 4 and 5 are averages for data collected for four sets of SAMs. The data points associated with 0.90 and 0.95 mole fraction of F8C11/C16 in solution was only collected for one set of SAMs.
- (50) For the ellipsometric data in Figure 6, error bars reflect the standard deviation for a data set comprising 18 measurements.
- (51) The dashed lines in Figures 5, 6, and 8 are the calculated linear fit trendlines associated with the first five data points in each of the figures using the “error as weight” function. These plots were produced in OriginPro 7.5.
- (52) Tamada, K.; Ishida, T.; Knoll, W.; Fukushima, H.; Colorado, R., Jr.; Graupe, M.; Shmakova, O. E.; Lee, T. R. Molecular packing of semifluorinated alkanethiol self-assembled monolayers on gold: Influence of alkyl spacer length. *Langmuir* **2001**, *17*, 1913–1921.
- (53) Laibinis, P. E.; Nuzzo, R. G.; Whitesides, G. M. Structure of monolayers formed by coadsorption of two n-alkanethiols of different chain lengths on gold and its relation to wetting. *J. Phys. Chem.* **1992**, *96*, 5097–5105.
- (54) Snyder, R. G.; Hsu, S. L.; Krimm, S. Vibrational spectra in the carbon-hydrogen stretching region and the structure of the polymethylene chain. *Spectrochim. Acta, Part A* **1978**, *34A*, 395–406.
- (55) MacPhail, R. A.; Strauss, H. L.; Snyder, R. G.; Elliger, C. A. Carbon-hydrogen stretching modes and the structure of n-alkyl chains. 2. Long, all-trans chains. *J. Phys. Chem.* **1984**, *88*, 334–341.
- (56) For the PM-IRRAS data in Figure 7, error bars reflect the standard deviation for four sets of data.
- (57) Morra, M.; Occhiello, E.; Garbassi, F. Knowledge about polymer surfaces from contact angle measurements. *Adv. Colloid Interface Sci.* **1990**, *32*, 79–116.
- (58) Johnson, R. E., Jr.; Dettre, R. H. In *Surface and Colloid Science*; Matijevic, E., Ed.; Wiley-Interscience: New York, 1969; Vol. 2, pp 85–153.
- (59) Colorado, R., Jr.; Lee, T. R. Physical organic probes of interfacial wettability reveal the importance of surface dipole effects. *J. Phys. Org. Chem.* **2000**, *13*, 796–807.
- (60) For the contact angle data in Figure 8, error bars reflect the standard deviation for three sets of data.
- (61) Krafft, M. P. Fluorocarbons and fluorinated amphiphiles in drug delivery and biomedical research. *Adv. Drug Delivery Rev.* **2001**, *47*, 209–228.
- (62) Krafft, M. P. Large organized surface domains self-assembled from nonpolar amphiphiles. *Acc. Chem. Res.* **2012**, *45*, 514–524.
- (63) *Handbook of Surface and Colloid Chemistry*; Birdi, K. S., Ed.; CRC Press: Boca Raton, FL, 1997.
- (64) Israelachvili, J. N. *Intermolecular & Surface Forces*, 2nd ed.; Academic Press: London, 1991.
- (65) Malone, S. M.; Trabelsi, S.; Zhang, S.; Lee, T. R.; Schwartz, D. K. Self-assembly of linactants: micelles and lyotropic liquid crystals in two dimensions. *J. Phys. Chem. B* **2010**, *114*, 8616–8620.
- (66) Nelson, K. E.; Gamble, L.; Jung, L. S.; Boeckl, M. S.; Naeemi, E.; Golledge, S. L.; Sasaki, T.; Castner, D. G.; Campbell, C. T.; Stayton, P. S. Surface characterization of mixed self-assembled monolayers designed for streptavidin immobilization. *Langmuir* **2001**, *17*, 2807–2816.
- (67) Riepl, M.; Enander, K.; Liedberg, B.; Schaeferling, M.; Kruschina, M.; Ortigao, F. Functionalized surfaces of mixed alkanethiols on gold as a platform for oligonucleotide microarrays. *Langmuir* **2002**, *18*, 7016–7023.
- (68) Yang, W. R.; Hibbert, D. B.; Zhang, R.; Willett, G. D.; Gooding, J. J. Stepwise synthesis of Gly-Gly-His on gold surfaces modified with mixed self-assembled monolayers. *Langmuir* **2005**, *21*, 260–265.
- (69) Ishii, N.; Fitrilawati, F.; Manna, A.; Akiyama, H.; Tamada, Y.; Tamada, K. Gold nanoparticles used as a carrier enhance production of anti-hapten IgG in rabbit: a study with azobenzene-dye as a hapten presented on the entire surface of gold nanoparticles. *Biosci., Biotechnol., Biochem.* **2008**, *72*, 124–131.